ACTA IMEKO
ISSN: 2221-870X
June 2025, Volume 14, Number 2, 1 - 6

Statistical analysis of the angle of linear polarization for the winding angle measurement in carbon fibre components

Luciano Chiominto[1], Giulio D'Emilia[1], Emanuela Natale[1]

[1] *DIIIE, Università degli Studi dell'Aquila, 67100 L'Aquila, Italy*

ABSTRACT
In this work, the problem of determining the winding angle in a cylindrical carbon fiber piece, obtained through a filament winding process, is investigated. A polarization camera is used for the measurement, and the winding angle is determined by statistically analyzing the angle of linear polarization in each pixel of the region under study. The main influence parameters are considered, like non-planarity and superficial state of the piece, with the aim of reducing the measurement uncertainty. For this purpose, two different types of data processing approaches are tested and compared.

Section: RESEARCH PAPER

Keywords: polarized camera; uncertainty; composite materials; carbon fibre; defect inspection; AoLP; angle measurement

Citation: L. Chiominto, G. D'Emilia, E. Natale, Statistical analysis of the angle of linear polarization for the winding angle measurement in carbon fibre components, Acta IMEKO, vol. 14 (2025) no. 2, pp. 1-6. DOI: 10.21014/actaimeko.v14i2.2065

Section Editor: Laura Fabbiano, Politecnico di Bari, Italy

Received January 31, 2025; **In final form** June 7, 2025; **Published** June 2025

Funding: National Italian project "Smart Tow Winding – Nuove soluzioni ad elevata automazione per l'impregnazione e l'avvolgimento di tow" – European Union, Fondo Europeo di Sviluppo Regionale, Project Code: ARS01_00871

Corresponding author: Luciano Chiominto, e-mail: luciano.chiominto@graduate.univaq.it

1. INTRODUCTION

Carbon fibre-reinforced polymers (CFRPs) have emerged as one of the most significant advancements in materials science, owing to their exceptional strength-to-weight ratio, corrosion resistance, and versatility in a wide range of fields [1], [2]. Many scientific papers explore the applications of CFRPs, examining their advantages, challenges, and recent innovations, as well as their potential for future technological advancements [3]-[6].

Different methods exist for producing composite materials, each suited to different types of composites and end-use applications. In particular, for the production of cylindrical constructions such as tanks or pipes, filament winding is one of the most efficient and promising manufacturing methods [7]-[9]. In order to create an axially symmetric structure, this method entails wrapping continuous filaments coated with resin, according to predefined patterns, around a revolving mandrel. The fibre orientation and lay-up sequences can be tailored to achieve optimal mechanical properties in the finished product, such as high strength and stiffness in specific directions. Filament winding is particularly advantageous for producing components in aerospace and automotive industries where weight reduction and structural integrity are paramount. In these cases, the winding angle is a critical parameter that influences the mechanical characteristics of the final component [10], [11], so suitable and effective inspection methods are required for product quality control, possibly already during the production phase [12], [13].

Vision-based techniques provide a number of benefits over traditional inspection methods, including simplicity of automation, low cost, and the absence of contact [14]-[17]. The algorithms used for image processing are a crucial component of the whole inspection system.

One of the most advanced vision-based techniques for inspecting carbon fibre components is based on polarization imaging, that reveals the polarization condition of reflected light. In particular, in composite components, carbon fibres demonstrate to reflect unpolarized light in a polarized way, according to the same angle of the fibre orientation [1], [8], [18], [19].

This physical phenomenon allows to determine one-shot the angles of the carbon fibres in the imaged area, using processing algorithms that, in their basic form, are quite simple and fast to apply.

Of course, polarization imaging requires specialized cameras that can capture images at different polarization angles,

equipped with polarizing micro-filters that selectively allow only light of a certain polarization direction to pass through.

However, the technique is affected by some sources of uncertainty such as the surface state of the material, the curvature of the surface (if it is, for example, a cylindrical surface), as well as the variability of the illumination, or vibrations.

This study aims to investigate possible processing approaches for enhancing winding angle measurement on a carbon fibre cylinder, by a polarized vision system. The main influence parameters will be considered, like non-planarity and superficial state of the piece, with the aim of reducing the measurement uncertainty.

2. MATERIALS AND METHODS

The monochrome polarized camera FLIR Blackfly S BFS-PGE-51S5P is used, based on the Sony IMX 250 CMOS sensor. The camera has a native resolution of 2448 × 2048 pixels.

Each squared group of four pixels is equipped with four-direction (0°, 45°, 90°, 135°) polarizers, so four different orientations of light polarization information may be acquired simultaneously.

The lighting system consists of two soft-boxes with 80 W light bulbs, that produce a diffused and unpolarized light (Figure 1), and a 25 mm low-distortion lens is employed.

Other settings are as follows:

- 190 mm: camera-piece distance;
- 400 mm: softboxes-piece distance;
- 150 ms: exposure time;
- *f*/8: *f*-number.

The images are acquired using the Spinnaker SpinView acquisition program and saved in RAW format; MATLAB is then used to process the data.

A hollow cylinder representing a portion of a pressure vessel is used as the specimen for analysis (Figure 1). It is constituted of the following materials produced by Huntsman Araldite [9]:

- Araldite LY 3508 as epoxy resin.
- Aradur 1571 as hardener.
- Accelerator 1573 as accelerator.

Figure 1. Experimental setup.

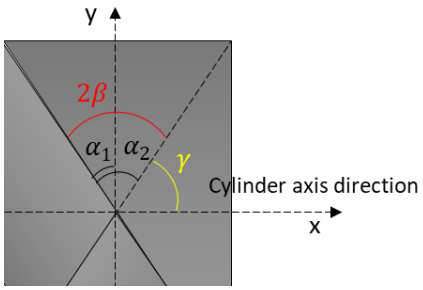

Figure 2. Definition of the winding angle γ.

The cylinder has an internal diameter of 200 mm and a length of 300 mm, and the texture is characterized by a nominal winding angle $\gamma = 60°$, defined as shown in Figure 2.

α_1 and α_2 are the inclination angles of the two carbon fibre tows with respect to the y-axis in the figure, theoretically equal in modulus to 30° and of opposite sign if measured clockwise with respect to the y-axis, while γ is complementary to 30°, therefore nominally equal to 60°, as said.

The method used in this work involves measuring the tow angles α_1 and α_2, the difference of which gives $2\,\beta$. The winding angle is, finally, obtained by subtracting β from 90° (Figure 3).

2.1. Data processing methodology

The initial phase of processing is the "demosaicing", that, for every direction of polarization, extracts the intensity values: this step produces an image for every polarization direction, characterized by a fourth of the original image's resolution (1224 × 1024 pixels).

Next, the Stokes parameters [1] are calculated to characterize the light polarization state, taking into account the pixel intensity for each direction (I_0, I_{45}, I_{90}, I_{135}):

$$S_0 = \frac{I_0 + I_{45} + I_{90} + I_{135}}{2\,L} \tag{1}$$

$$S_1 = I_0 - I_{90} \tag{2}$$

$$S_2 = I_{45} - I_{135}\,. \tag{3}$$

Finally, the Angle of Linear Polarization (AoLP) is calculated using the following formula:

$$AOLP = 0.5 \cdot \operatorname{atan}\left(\frac{S_2}{S_1}\right). \tag{4}$$

This processing stage yields a matrix 1224 × 1024, where each element represents the AoLP value in each pixel. These data, ranging in the interval [-90°; 90°], correspond to the fibre orientation in each pixel of the image.

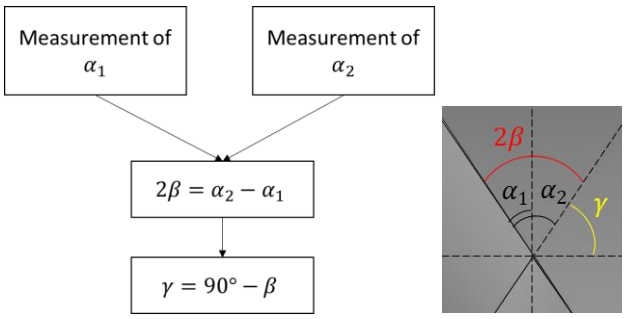

Figure 3. Indirect γ measurement methodology.

Theoretically, for each image the AoLP values are distributed according to a bimodal distribution. This since in the examined case there are two nominal orientations of the tows. Fitting the frequency histograms of the AoLP values with two distributions, it is possible to estimate α_1 and α_2 as the means of the two distributions itself [20]. In this work, the frequency values are fitted considering Gaussian and Lorentzian distributions. The goodness of fitting is assessed considering the coefficient of determination or R^2 statistic.

The standard deviation of these distributions can be related to the irregularity of the surface (fibre orientation, layer of resin, curvature), but also to the variability of the method itself.

To reduce the effect of the curvature, a method has been developed in a previous work of the authors, which allows to identify the Region of Interest (RoI) in which this effect is limited to a value considered acceptable [21].

To evaluate the tows angles, the dataset is split into two parts. One for positive AoLP values and the other for negative ones.

In this work, to reduce the measurement variability, twenty AoLP images are acquired successively in repeatable conditions, leaving the cylinder and the camera in the same position. Then, on the basis of these twenty images, the following processing techniques are developed and compared:

Method 1: averaging, pixel by pixel, of the twenty AoLP images, to get a single AoLP image. Then, with reference to this averaged image, determination of the α_1 and α_2 angles from the fitted distributions, as described.

Method 2: determination of the α_1 and α_2 angles from the fitted distributions, for each of the twenty acquired images. Then, calculation of the means of the n values obtained for both α_1 and α_2.

3. RESULTS

The preliminary processing steps (demosaicing, Stokes parameter calculation and, finally, AoLP matrix determination) have been performed as described in Section 2.1. Furthermore, the RoI on which to carry out the analysis has been identified as described in [21], to minimize the effect of the surface curvature.

In this section, the results obtained using a Gaussian fitting are reported. The comparison between Gaussian and Lorentzian distribution is discussed in Section 4.

The results of these first steps are described in Figure 4, which shows the colour map of the AoLP, and the corresponding relative frequencies in the RoI, fitted by two Gaussian distributions: these results have been obtained for each of the twenty images acquired.

3.1. Method 1

The results of the application of Method 1 are shown in Figure 5, which represents the distribution of the relative frequencies of the AoLP in the image obtained by averaging, pixel by pixel, the twenty acquired images. In the same figure, the two Gaussians that fit the experimental data is also depicted. The values of α_1 and α_2 are, therefore, estimated by identifying the average values of the two Gaussians, equal, respectively, to -33.3° and 34.5°. The standard deviations of the fitted distributions are 8.7° and 5.6°, respectively. These standard deviations refer to the variability of the angle on all the pixels of the averaged image. The winding angle, applying the procedure described in Figure 3, results equal to $\gamma = 56.1°$.

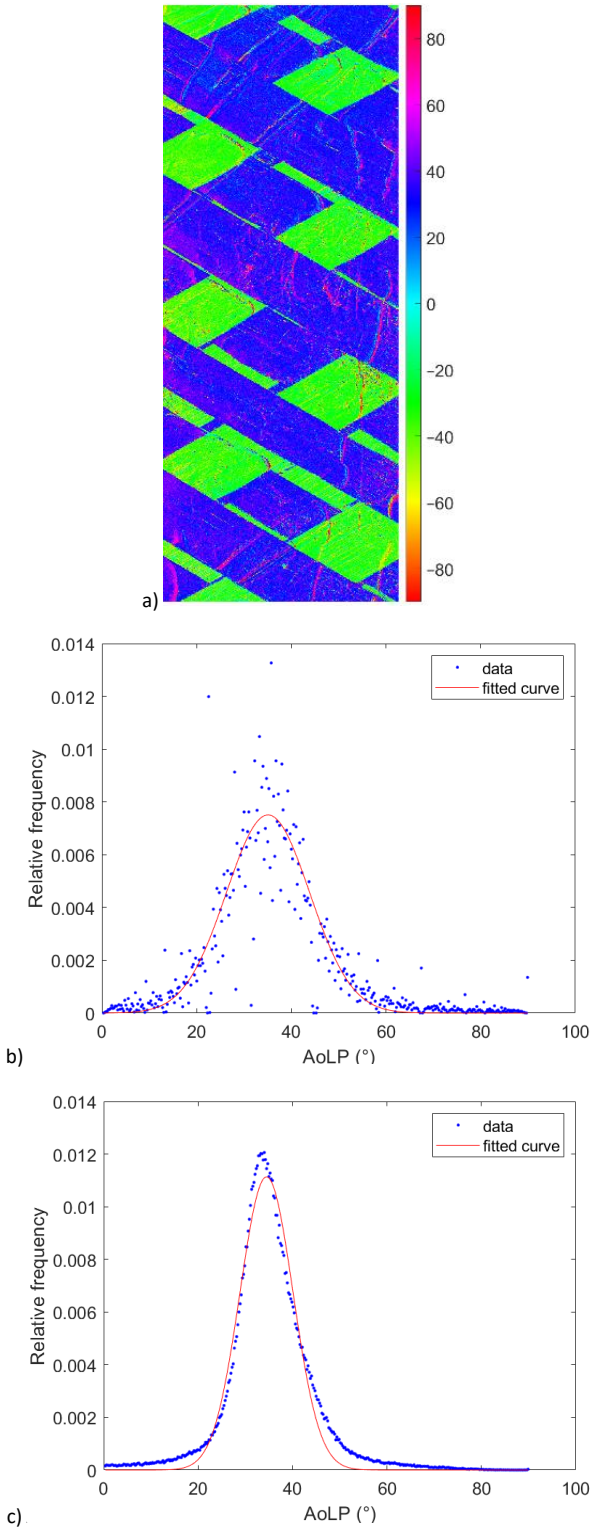

Figure 4. Results of the preliminar processing of the image: a) Colour map of the RoI of the AoLP image; b) Fitting of the positive AoLP distributions; c) Fitting of the negative AoLP distributions.

It is noted that the two angles α_1 and α_2, that theoretically are equal in modulus at 30° and of opposite sign, actually differ in modulus from each other by 1.2°, if the described averaging procedure is applied.

In Figure 6, the effect of the image averaging on the mean values and standard deviations for α_1 and α_2 are reported. In each step an image is added to the previous ones.

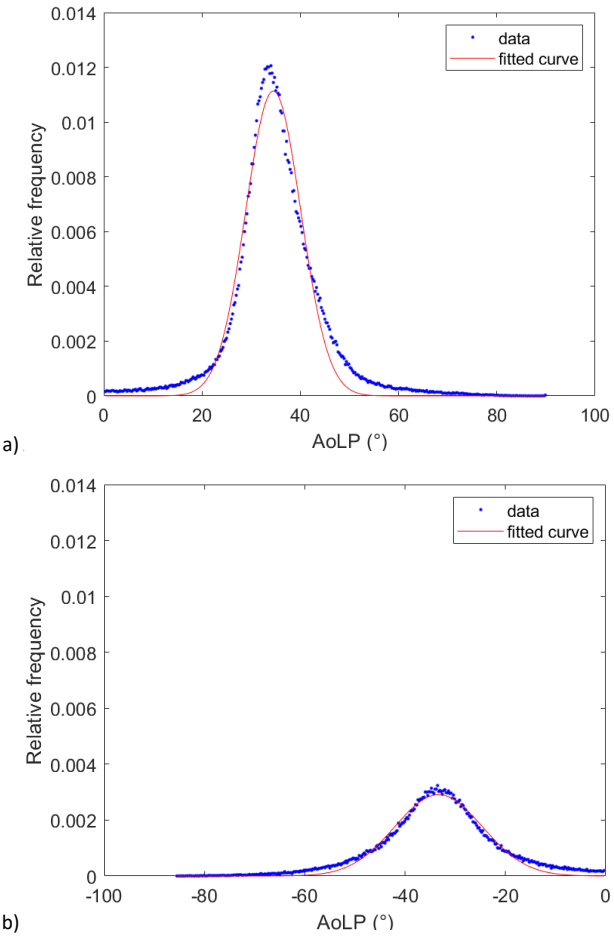

Figure 5. AoLP relative frequency distributions and fitted Gaussians on the pixel-by-pixel averaged image.

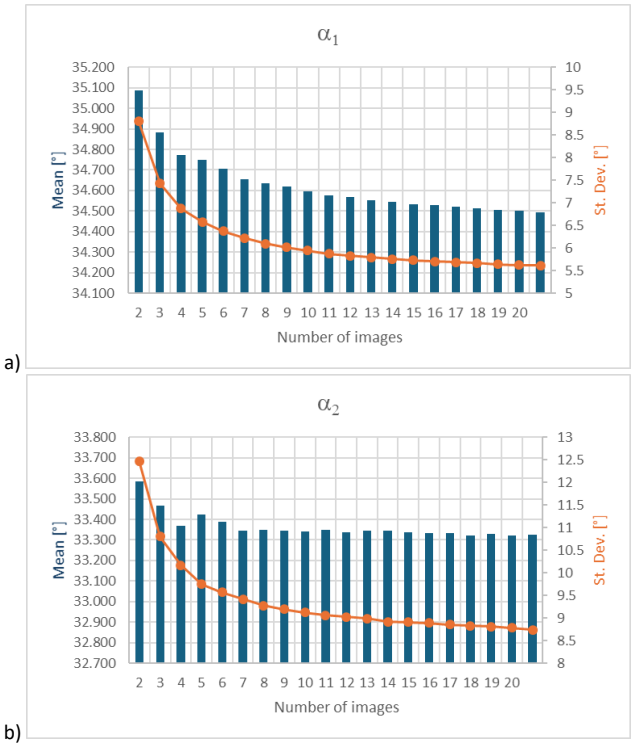

Figure 6. Trend of absolute mean value (blue columns) and standard deviation (orange line) of the Gaussian distribution, varying the number of images on which the image is averaged, pixel by pixel: a) for α_1 angle; b) for α_2 angle.

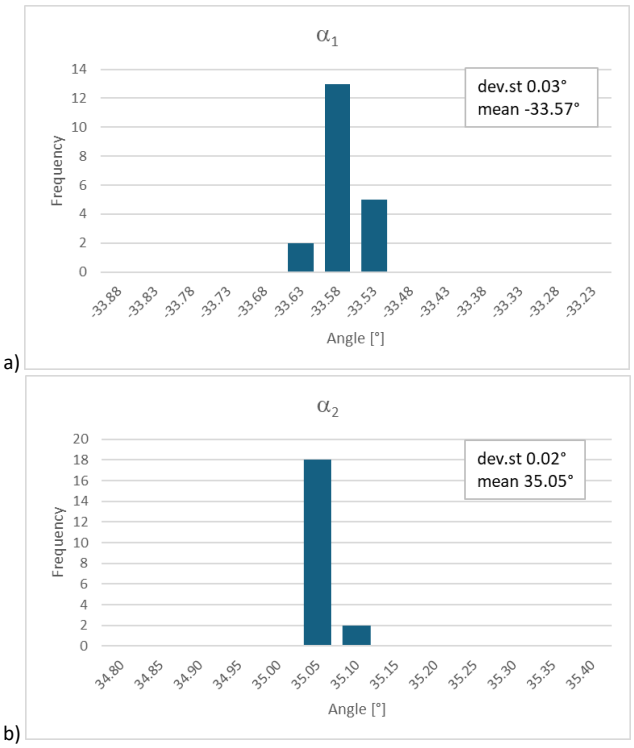

Figure 7. Frequency histogram of measured tow angles α_1 (a) and α_2 (b) on twenty different images.

As shown in Figure 6, averaging pixel by pixel an increasing number of images has two main effects:

- Reduction of the standard deviation of the fitted Gaussians
- Reduction of the mean value of the fitted Gaussian.

Considering the standard deviation trend, in the beginning there is a sharp decrease in the variability, adding images. This procedure lowers the variability of the fitted Gaussians, due to the reduction of noise.

As for the mean value, this reduction trend is more noticeable in the α_1 angle where it decreases of about 0.5°. It starts from 35° in the first image, and it is equal to 34.5° after averaging all the acquisitions in the dataset. At the same time, α_2 has a minor reduction in the mean value that can be considered constant during this procedure.

It is also observed that the averaging procedure, pixel by pixel, presupposes a correspondence of the pixels to precise points of the object in the successive acquisitions. This assumption is not always guaranteed in practice, when significant levels vibrations can occur, acting on the piece and/or on the camera itself: in these cases, if vibration-damping supports cannot be used, Method 2 is preferable.

3.2. Method 2

Method 2, as described, involves determining the α_1 and α_2 angles from the Gaussian distributions resulting in each of the twenty acquired images; then, the average is calculated on the twenty values obtained, for both α_1 and α_2.

The analysis of the α_1 and α_2 values obtained on the twenty images, produces the frequency histograms shown in Figure 6: it can be seen that the mean of α_1 and α_2 are, respectively, equal to -33.6° and 35.1°, while the standard deviations are, correspondingly, equal to 0.03° and 0.02°. The winding angle, applying the procedure described in Figure 3, results equal to

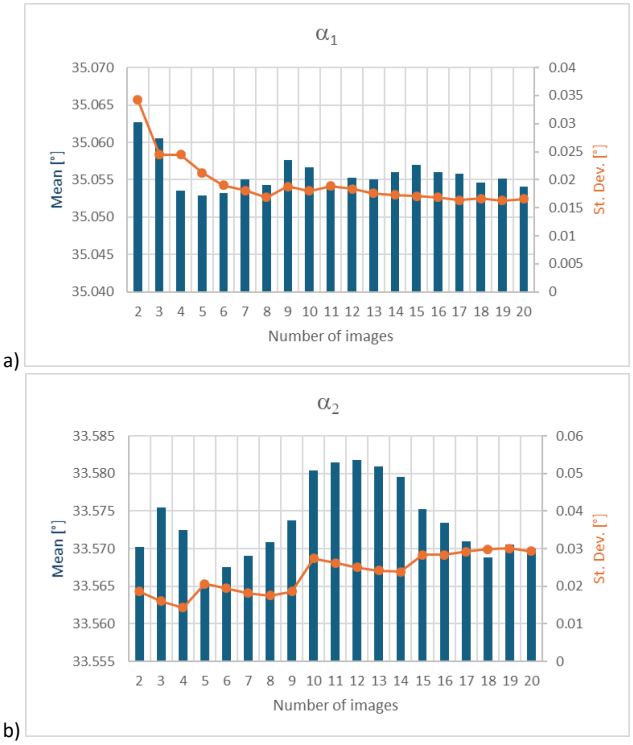

a)

b)

Figure 8. Trend of absolute mean value (blue columns) and standard deviation (orange line), varying the number of images on which they are calculated: a) for α_1 angle; b) for α_2 angle.

$\gamma = 55.7°$. The modulus estimates of α_1 and α_2, as can be also seen in Figure 7, are characterized by low variability, with standard deviations less than 1 %. Furthermore, the mean values appear closer in modulus than in the case of the results of Method 1, differing by 1.5°.

If we analyse how the absolute mean values and standard deviations vary by increasing the number of values on which the calculations are performed, from 2 to 20, the trends in Figure 8 are obtained.

From the analysis of these graphs, we note that the means remain stable going from 2 to 20 images, varying less than 0.1 %. Similarly, the standard deviations are in the order of around a few hundredths of a degree.

It is also interesting to note that the two Gaussian distributions in the individual images have a standard deviation of 12.5° and 8.8°, with reference to α_1 and α_2, respectively: these values are higher than the standard deviations of the Gaussians obtained on the pixel-by-pixel averaged image (8.7° and 5.6°). It is evident that the averaging operation on the single pixel allows to lower the variability of the AoLP angles in the resulting image.

4. DISCUSSION

With a nominal winding angle γ of 60°, the two methods, Method 1 and Method 2, provide the values for γ of 56.1° and 55.7°, respectively. There is a slight asymmetry between the absolute values of the angles α_1 and α_2, which differ by 1.2° in the case of Method 1, and 1.5° in the case of Method 2.

In Method 1, the standard deviation of the two Gaussians that fit the experimental relative frequencies, and equal to 8.7° and 5.6°, respectively, are representative of the variability in the entire image, and are related to the variability in the orientation of the fibres, but also to irregularities in the resin layer and the surface shape. This variability is, therefore, not directly comparable with the standard deviation of the twenty α_1 and α_2 values obtained with Method 2 (0.03° and 0.02°, respectively), which, instead, represent a repeatability uncertainty inherent to the method.

The methods provide comparable results, if we consider the calculated winding angle, equal to 56.1° in the case of Method 1, and 55.7° in the case of Method 2.

The suitability of fitting the AoLP frequencies using Gaussian and Lorentzian distributions has been assessed. The coefficient of determination shows similar results for the two distributions. It reaches 0.98 when the AoLP frequencies are obtained by averaging different images (Methods 1), while it reduces to 0.7 considering a single AoLP image.

Moreover, compared to the Gaussian fitting, using a Lorentzian distribution shows differences of no more than 0.1° in the winding angle (γ). Considering Method 2, the differences between the results are negligible.

Method 1 could be more susceptible to environmental vibrations, since the pixel-by-pixel average theoretically presupposes the exact correspondence of pixels with precise points on the object: this aspect, therefore, should be kept under control.

Furthermore, the angle values obtained have been compared with the measurement results obtained by applying an edge detection method on images acquired with a traditional camera [9], and the values have been found to be compatible, i.e. different by an amount lower than the expanded uncertainty (95 % confidence level).

In the development of the work, a flat piece of carbon fibre manufactured with great accuracy will be used as a reference for the evaluation of any systematic effects, and of the measurement uncertainty, and, in particular, to quantify the impact of surface finish and curvature of the material.

5. CONCLUSIONS

In this work, the problem of determining the winding angle in an axisymmetric carbon fibre piece, obtained through a filament winding process, has been investigated.

A polarization camera has been used for angle evaluation, and two different types of data processing approaches have been tested.

In the first case, twenty AoLP images have been averaged pixel by pixel, and the fibre angles have been determined by identifying the means of the two Gaussian distributions that fit the experimental frequencies.

In the second approach, for each of the twenty AoLP images, the fibre angles have been determined from the Gaussian distributions and, finally, the twenty values have been averaged.

The methods provide comparable results, if we consider the indirectly measured winding angle, equal to 56.1° in the case of Method 1, and 55.7° in the case of Method 2, and the corresponding variability.

In future work the investigation methods will be applied on a piece that could be considered as a reference, due to the regularity of the fibre angles, the flatness and the surface finish, to identify any systematic errors and evaluate the uncertainty inherent to the measurement method. The results of this study will provide information to identify specific precautions and solutions to improve the technique, or to allow us a more accurate delimitation of its applicability to practical cases.

Finally, it is emphasized that the technique, in its current configuration, is suitable for the analysis of flat, cylindrical, and spherical surfaces, thanks to the RoI identification method that minimizes the curvature effect. Modifications to the experimental setup and the data processing algorithm will be studied to evaluate its possible extension to more complex geometries.

AUTHORS' CONTRIBUTION

Conceptualization, G.D., L.C. and E.N; methodology, G.D., L.C. and E.N.; software, L.C.; validation, L.C., E.N. and G.D.; formal analysis, E.N. and L.C.; investigation, L.C. and E.N.; resources, G.D.; data curation, L.C.; writing original draft preparation E.N; writing review and editing, G.D. and L.C.; visualization, L.C. and E.N.; supervision, G.D.; project administration, G.D.; funding acquisition, G.D.

REFERENCES

[1] G. A. Atkinson, S. O'Hara Nash, L. N. Smith, Precision Fiber Angle Inspection for Carbon Fiber Composite Structures Using Polarisation Vision, Electronics 10 (2021), 2765. DOI: 10.3390/electronics10222765

[2] M. Schöberl, K. Kasnakli, A. Nowak, Measuring Strand Orientation in Carbon Fiber Reinforced Plastics (CFRP) with Polarization, Proc. of the World Conference on Non-Destructive Testing, Munich, Germany, 13–17 June 2016. Online [Accessed 12 June 2025] https://www.ndt.net/article/wcndt2016/papers/p20.pdf

[3] A. Sayam, A. M. Rahman, M. S. Rahman, S. A. Smriti, F. Ahmed, M. F. Rabbi, ... M. O. Faruque, A review on carbon fiber-reinforced hierarchical composites: mechanical performance, manufacturing process, structural applications and allied challenges, Carbon Lett. 32 (2022), 1173-1205. DOI: 10.1007/s42823-022-00358-2

[4] C. G. Naidu, C. V. Ramana, Y. S. Rao, K. V. P. Rao, D. Vasudha, G. Anusha, K. B. Rajeshbabu, A Concise Review on Carbon Fiber-Reinforced Polymer (CFRP) and Their Mechanical Significance Including Industrial Applications, Carbon Nanotubes-Recent Advances, New Perspectives and Potential Applications, 2023 DOI: 10.5772/intechopen.109339

[5] Y. Luo, Z. Shi, S. Qiao, (+ another 8 authors), Advances in nanomaterials as exceptional fillers to reinforce carbon fiber-reinforced polymers composites and their emerging applications, Polym. Compos., 2024. DOI: 10.1002/pc.29027

[6] G. Liu, Y. Xiong, L. Zhou, Additive manufacturing of continuous fiber reinforced polymer composites: Design opportunities and novel applications, Compos. Commun. 27 (2021), 100907. DOI: 10.1016/j.coco.2021.100907

[7] M. Azeem, H. H. Ya, M. A. Alam, M. Kumar, P. Stabla, M. Smolnicki, M. Mustapha, Application of Filament Winding Technology in Composite Pressure Vessels and Challenges: A Review, J. Energy Storage 49 (2022), 103468. DOI: 10.1016/j.est.2022.103468

[8] M. B. Antunes, J. H. S. Almeida Jr., S. C. Amico, Curing and Seawater Aging Effects on Mechanical and Physical Properties of Glass/Epoxy Filament Wound Cylinders, Compos. Commun. 22 (2020), 100517. DOI: 10.1016/j.coco.2020.100517

[9] E. Natale, A. Gaspari, L. Chiominto, G. D'Emilia, A. G. Stamopoulos, Morphological Analysis of As-Manufactured Filament Wound Composite Cylinders Using Contact and Non-Contact Inspection Methods, Eng. Fail. Anal. 158 (2024), 108011. DOI: 10.1016/j.engfailanal.2023.108011

[10] T. Yokozeki, T. Ogasawara, T. Ishikawa, Effects of Fiber Nonlinear Properties on the Compressive Strength Prediction of Unidirectional Carbon–Fiber Composites, Compos. Sci. Technol. 65 (2005), pp. 2140-2147. DOI: 10.1016/j.compscitech.2005.05.024

[11] K. M. Subhedar, G. S. Chauhan, B. P. Singh, S. R. Dhakate, Effect of Fiber Orientation on Mechanical Properties of Carbon Fiber Composites, Indian J. Eng. Mater. Sci. 27 (2021), pp. 1100-1103.

[12] R. Gupta, D. Mitchell, J. Blanche, S. Harper, W. Tang, K. Pancholi, D. Flynn, A Review of Sensing Technologies for Non-Destructive Evaluation of Structural Composite Materials, J. Compos. Sci. 5 (2021), 319. DOI: 10.3390/jcs5110319

[13] G. D'Emilia, A. Di Ilio, A. Gaspari, E. Natale, A. G. Stamopoulos, L. Chiominto, Vision System for Optical Quality Control of Components Made by Fibre Thermoplastic-Based Composites, Proc. of the 2021 IEEE Int. Workshop on Metrology for Industry 4.0 & IoT (MetroInd4.0&IoT), Rome, Italy, 7–9 June 2021, IEEE, pp. 59-64. DOI: 10.1109/MetroInd4.0IoT51437.2021.9488498

[14] G. D'Emilia, A. Gaspari, E. Natale, D. Ubaldi, Uncertainty Evaluation in Vision-Based Techniques for the Surface Analysis of Composite Material Components, Sensors 21 (2021), 4875. DOI: 10.3390/s21144875

[15] S. Zhong, W. Nsengiyumva, Visual testing for fiber-reinforced composite materials, in: Nondestructive Testing and Evaluation of Fiber-Reinforced Composite Structures, Springer Nature Singapore, Singapore, 2022, pp. 97–132. DOI: 10.1007/978-981-19-0568-3_5

[16] A. Maghami, M. Salehi, M. Khoshdarregi, Automated vision-based inspection of drilled CFRP composites using multi-light imaging and deep learning, CIRP Journal of Manufacturing Science and Technology 35 (2021), pp. 441–453. DOI: 10.1016/j.cirpj.2021.08.014

[17] S. Fotouhi, F. Pashmforoush, M. Bodaghi, M. Fotouhi, Autonomous damage recognition in visual inspection of laminated composite structures using deep learning, Composite Structures 268 (2021), Article 113960. DOI: 10.1016/j.compstruct.2021.113960

[18] G. A. Atkinson, T. J. Thornton, D. I. Peynado, J. D. Ernst, High-Precision Polarization Measurements and Analysis for Machine Vision Applications, Proc. of the 2018 7th European Workshop on Visual Information Processing (EUVIP), Tampere, Finland, 26–28 November 2018, pp. 1-6. DOI: 10.1109/EUVIP.2018.8611711

[19] D. Schommer, M. Duhovic, T. Hoffmann, J. Ernst, K. Schladitz, A. Moghiseh, K. Steiner, Polarization Imaging for Surface Fiber Orientation Measurements of Carbon Fiber Sheet Molding Compounds, Compos. Commun. 37 (2023), 101456. DOI: 10.1016/j.coco.2023.101456

[20] L. Chiominto, G. D'Emilia, E. Natale, Using Light Polarization to Identify Fiber Orientation in Carbon Fiber Components: Metrological Analysis, Sensors, 24(17), 2024, 5685. DOI: 10.3390/s24175685

[21] L. Chiominto, G. D'Emilia, E. Natale, F. Tiberi, Optical analysis of composite materials: metrological issues, XXXII AIVELA National Meeting, December 2024.